Multivariate Linear Models for In Situ Monitoring of Low-Activity Nuclear Waste Using Infrared and Raman Spectroscopy – 20218

Stefani Kocevska *, Ronald W. Rousseau *, Martha A. Grover *, Giovanni Maria Maggioni *
* Georgia Institute of Technology

ABSTRACT

This paper presents the use of *in situ* monitoring tools for molecular analysis of non-radioactive species found in the supernatant liquid and dissolvable saltcake of nuclear waste at Hanford. We have selected two *in situ* spectroscopic techniques that do not require any sample preparation or consumables: infrared (in the form of attenuated total reflectance Fourier transform infrared or ATR-FTIR) and Raman spectroscopy. This work aims to evaluate their performance for liquid waste simulants representative of the Hanford DFLAW (Direct Feed Low-Activity Waste) feed. In addition, we have evaluated the performance of four multivariate linear models that extract concentrations from spectral measurements for a data set that was designed to include key molecular species found in liquid low-activity waste.

INTRODUCTION

The Hanford Site in Washington State stores approximately 55 million gallons of nuclear and chemical waste that originated from the production of plutonium as part of the Manhattan Project. In general, the waste is categorized in three types: supernatant liquid, saltcake solids, and sludge. The supernatant liquid and the dissolvable saltcake have been classified as low-activity waste (LAW) that contains small amounts of radionuclides, while the water-insoluble sludge is classified as high-level waste (HLW). Under the current timeline, vitrification of the low-activity waste will be implemented first. Remediation efforts are expected to continue for another 50 years. The goal is to immobilize all waste in a borosilicate glass form, which will be cast in stainless steel canisters. [1–3]

The majority of the waste at Hanford falls under the LAW classification. The DOE has initiated the Direct Feed Low-Activity Waste (DFLAW) project to expedite clean-up of low-activity waste. DFLAW aims to vitrify supernatant low-activity waste, as shown in Figure 1. The initial steps include feeding the waste into the Tank Side Cesium Removal (TSCR) facility to reduce ^{137}Cs levels and remove insoluble solids. The preprocessed waste will be sent to the Waste Treatment and Immobilization Plant (WTP) for vitrification. The waste will be mixed with Glass-Forming Chemicals (GFCs) to create a melter feed slurry, which will be fed to a melter that operates at high temperatures to convert the feed to glass. Secondary waste, such as the Submerged Bed Scrubber (SBS) condensate, will be treated in the Effluent Treatment Facility (ETF).

The overall glass formulation depends on the composition of the waste. The complexity of the waste and its hazardous nature call for extensive sampling at different locations across DFLAW to facilitate processing. The Real-Time In-Line (RTIM) initiative seeks to reduce or replace existing offline sampling techniques with *in situ* monitoring, which can help minimize sample turn-around time. Online monitoring will also help reduce employee exposure to radiation and other hazards associated with collecting samples for offline analysis. [4–7] The liquid low-activity waste feed is made-up of more than 20 non-radioactive species, primarily sodium salts dissolved in water. Our research addresses online identification and quantification of these species using ATR-FTIR and Raman spectroscopy.

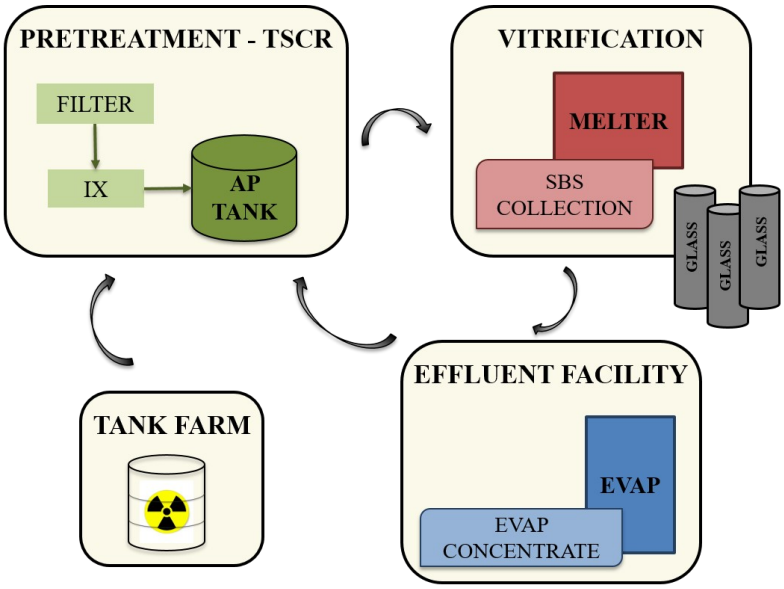

Figure 1: DFLAW - plan for direct vitrification of liquid low-activity waste at the Hanford site.

METHODS

Spectroscopic Methods

In our research we use two spectroscopic methods, infrared (ATR-FTIR) and Raman spectroscopy. Absorption spectroscopy, such as ATR-FTIR**,** occurs when a molecule absorbs light. [8,9] A molecule is IR-active if there is a change in the dipole moment during molecular vibrations, which generates a field that can interact with the electric field from light radiation. Energy is absorbed if the natural frequency of the vibration matches the frequency of the radiation. Scattering spectroscopy, such as Raman spectroscopy (inelastic scattering), occurs when the light radiation is scattered by matter. In Raman spectroscopy, the light radiation exchanges energy with the molecule, which results in a shift in the scattered radiation, known as the Raman effect [9]. Raman-active molecules exhibit changes in polarizability. In the case when molecular bonds are electrically symmetrical, they do not absorb infrared energy and are thus IR-inactive, but they can still be detected using Raman spectroscopy. Similarly, molecules that are weakly polarizable may be Raman-inactive but IR-active. The two techniques could be used simultaneously, which could be especially beneficial for multicomponent systems. The two techniques can also be used for verification and validation purposes if the species of interest are both IR and Raman active.

The intensity of the measured light radiation in both ATR-FTIR and Raman spectroscopy can be related to the concentration of the measured species. Assuming a linear dependence (which holds at low concentrations), the intensity can be expressed as a function of the concentration using the Beer-Lambert law:

$$X(\lambda) = \varepsilon(\lambda) l C \qquad 11\text{* MERGEFORMAT ()}$$

where $X(\lambda)$ is the intensity (a.u.), measured at each wavelength, $\varepsilon(\lambda)$ is the molar absorptivity (L mol^{-1} cm^{-1}) or molar attenuation coefficient, l is the path length (cm) and C is the concentration (mol solute/L solution). The measured intensity could also depend on the temperature or pH of the sample. This approach can be extended to mixtures of n spectroscopically active species using the superposition

rule, which assumes that the signal of a mixture can be determined by summing the individual signals of the pure components:

$$X(\lambda) = \sum_{i=1}^{n} \varepsilon_i(\lambda) C_i \qquad 22\backslash* \text{ MERGEFORMAT ()}$$

where $\varepsilon_i(\lambda)$ represents the molar attenuation coefficient of each component. The path length was dropped since it remains constant if the same instrument is used to collect measurements.

Chemometrics Methods

We selected four common chemometrics techniques to use in quantification of the composition of key analytes in nuclear waste. In Classical Least-Squares Regression (CLSR), [10–12] also known as the K-Matrix method, the molar attenuation coefficients are calculated using calibration data (subscript *c*) and stored in matrix **K**:

$$\mathbf{K} = \mathbf{C}_c^{-1}\mathbf{X}_c = (\mathbf{C}_c^{T}\mathbf{C}_c)^{-1}\mathbf{C}_c^{T}\mathbf{X}_c \qquad 33\backslash* \text{ MERGEFORMAT ()}$$

The coefficients from **K** can be used to analyze mixtures with unknown composition. The spectral intensity of an unknown mixture (subscript *m*) is defined as:

$$\mathbf{X}_m = \mathbf{K}\mathbf{C}_m \qquad 44\backslash* \text{ MERGEFORMAT ()}$$

Since $\mathbf{X}_m$ can be measured, the only unknown is the concentration $\mathbf{C}_m$, which can be calculated as:

$$\mathbf{C}_m = \mathbf{K}^{-1}\mathbf{X}_m = (\mathbf{K}^{T}\mathbf{K})^{-1}\mathbf{K}^{T}\mathbf{X}_m \qquad 55\backslash* \text{ MERGEFORMAT ()}$$

In this case, the number of wavelengths must be equal to or larger than the number of components. One of the main limitations of this method is the accuracy of the calibration set, which is affected by noise. The presence of noise may be misinterpreted as spectral activity, which will be stored in **K**. The calibration set should therefore include the active spectral region for each of the components to minimize the effect of noise. Other limitations include the assumption of linearity and superposition, of which the latter is affected by the extent of peak overlap.

Inverse Least-Squares Regression (ILSR), [10–12] also known as the P matrix method, is based on Beer-Lambert's law, but while CLSR models the spectral signal from information on the concentration and molar attenuation coefficients, ILSR uses the reverse approach to model the concentration as the product of the spectral signal and calibration coefficient matrix **P**:

$$\mathbf{C}_c = \mathbf{P}\mathbf{X}_c \qquad 66\backslash* \text{ MERGEFORMAT ()}$$

The coefficient matrix **P** is calculated from calibration data and relates the concentration of each component to the spectral signal at each wavelength:

$$\mathbf{P} = \mathbf{X}_c^{-1}\mathbf{C}_c = (\mathbf{X}_c^{T}\mathbf{X}_c)^{-1}\mathbf{X}^{T}\mathbf{C}_c \qquad 77\backslash* \text{ MERGEFORMAT ()}$$

In this case, the number of samples used in the calibration must be greater than the number of wavelengths used in $\mathbf{X}_c$. Once the coefficient matrix has been calculated, the concentration of an unknown mixture (subscript *m*) could be determined using:

$$\mathbf{C}_m = \mathbf{P}\mathbf{X}_m \qquad 88\backslash* \text{ MERGEFORMAT ()}$$

ILSR is limited by the accuracy of the calibration set and the selection of wavelengths. Using fewer wavelengths may minimize the effect of noise, but will not account for minor spectral features that differentiate overlapping peaks. On the other hand, increasing the number of samples will allow us to add more wavelengths to the model, but may lead to collinearities that result in correlated regression coefficients.

Data reduction, such as Principal Component Analysis (PCA) [11,13], is used to mitigate collinearity effects. PCA finds principal components that represent linear combinations of the original variables for a given observation. This is accomplished by projecting the original variables onto a new, smaller set of variables that are not correlated with each other. The magnitudes of the principal components (scores) $\mathbf{T}$ are defined as:

$$\mathbf{T} = \mathbf{X}\mathbf{P} \qquad 99\backslash* \text{ MERGEFORMAT ()}$$

where $\mathbf{P}$ stores the direction vectors of the principal components (loadings) and $\mathbf{X}$ is the original spectral matrix.

Principal Component Regression (PCR) is a technique that combines PCA with MLR [11,14]. First, the data set is reduced using PCA and then MLR is applied to regress the reduced set. Partial Least-Squares Regression (PLSR) is another regression tool that performs data reduction and regression simultaneously, utilizing both the independent and dependent data as input [11,14]. PLSR often has superior predictive power compared to PCR, because it considers the input-output relationship in the variable reduction. More detailed explanations and derivations of these algorithms can be found elsewhere [15,16].

Experimental Design

Simulated liquid waste mixtures were used to study the performance of ATR-FTIR and Raman spectroscopy. These mixtures were based on the LAWPS Cast Stone simulant that corresponds to pretreated liquid DFLAW feed [17]. For this work, we identified four species to study: $NaNO_3$, $NaNO_2$ and Na_2SO_4 due to their importance in DFLAW (nitrate and nitrite are present in abundance compared to other anions and sulfate interferes with the vitrification process) and Na_2CO_3 since the carbonate peak partially overlaps with the major peak of nitrate. Spectroscopic fingerprints of the four components are shown in Figure 2. Both the ATR-FTIR and Raman spectra were baselined using a background removal technique that minimizes a non-quadratic cost function, developed by Mazet et al. [18].

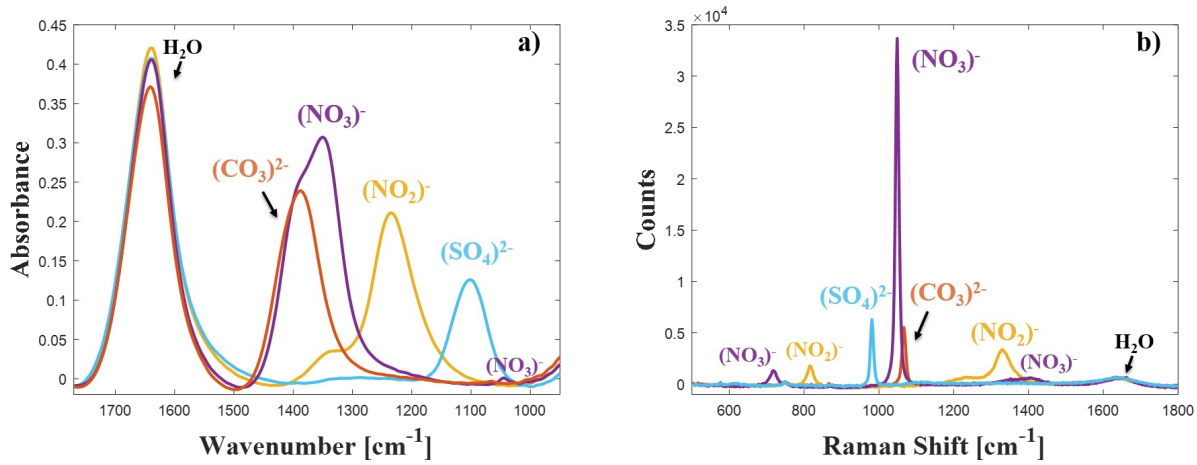

Figure 2: a) ATR-FTIR and b) Raman spectra of the components of interest for this work.

The calibration experiments were designed using a Faced Central Composite Design (CCF), which consisted of three levels (low, medium and high, based on the simulant recipe) for the four factors (species of interest). A full factorial design (3^4) that uses all possible combinations of levels for the factors would have required performing 81 experiments. The CCF design which includes using three levels for each factor (but not all the possible combinations) consisted of 36 experiments including replicates of the center point (medium level for all species) [19]. Spectra corresponding to the concentration levels are shown in Figure 3. The test set of unknown mixture concentrations of the same species was designed by interpolating and extrapolating from the training set. We measured the signal of 10 mixtures for the test set, shown in Figure 4.

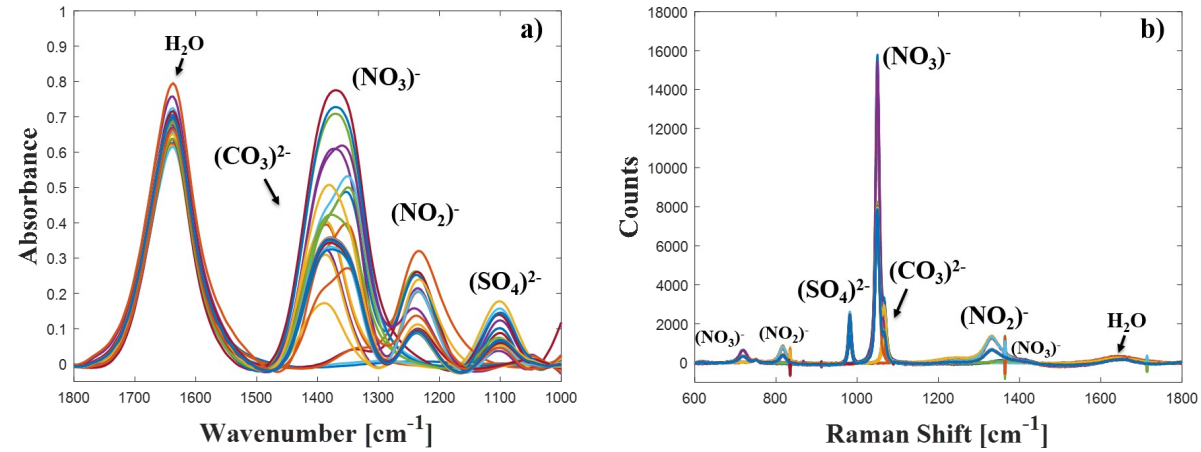

Figure 3: a) ATR-FTIR and b) Raman training data sets. A total of 36 baselined spectra are shown in each figure. The models were calibrated using the information provided here, coupled with the calibration concentration matrix.

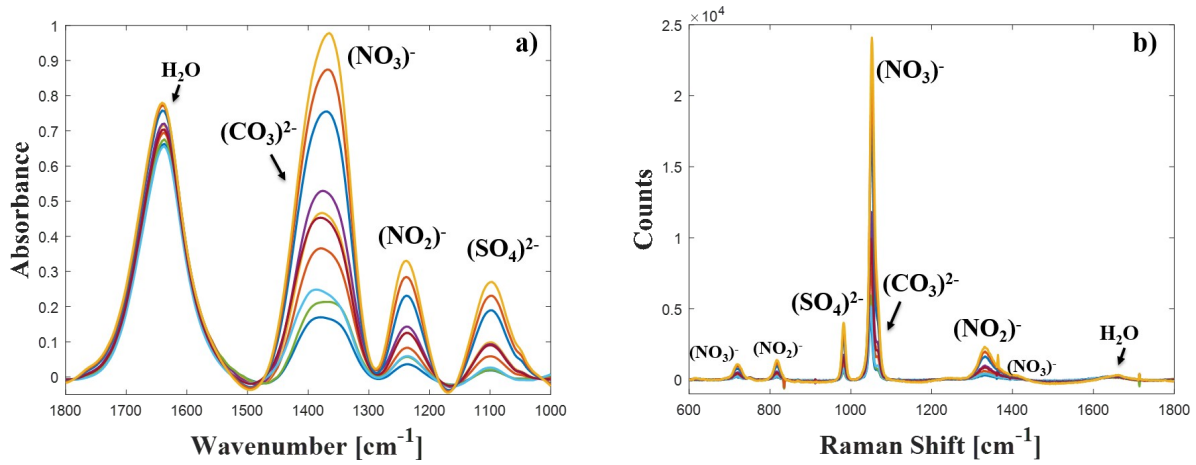

Figure 4: a) ATR-FTIR and b) Raman test data sets. These mixtures were generated by both interpolating and extrapolating the training data set, to test how the models perform in each case. A total of 10 unknown samples were collected.

DISCUSSION

The model comparison for both ATR-FTIR and Raman data sets is shown in Figure 5. The parity plots facilitate some general observations, as well as trends that vary for each spectroscopic technique. The first observation is that all four models begin to deviate from the parity line at higher concentrations, for both IR and Raman data. Another clear observation is that the ATR-FTIR predictions are much less accurate than those made using the same models on Raman data. Two possible explanations are peak overlap and sensitivity to baseline correction. IR spectra show a more pronounced overlap between the nitrate and carbonate peaks, as well as a partial overlap of nitrite with nitrate. The more pronounced overlaps, coupled with our baseline correction technique that aims to distinguish among peaks (which forces some non-zero peak heights to go to zero, such as the region between the nitrate and nitrite peak) has resulted in inaccurate estimates.

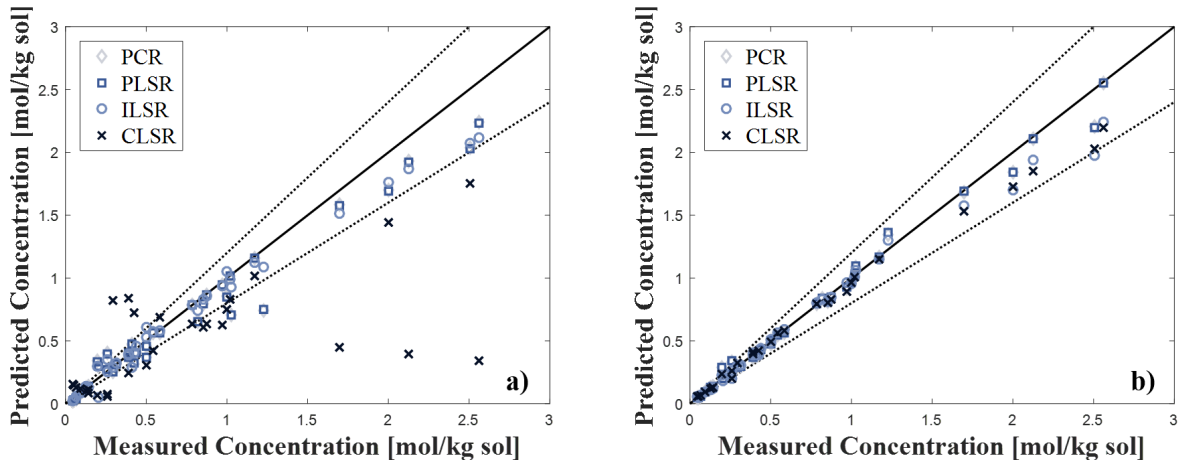

Figure 5: PCR, PLSR, ILSR and CLSR model predictions using a) ATR-FTIR and b) Raman data. The solid black line represents unity and the dashed black lines represents ±20% deviations, which are the acceptable limits at the Hanford analytical laboratory.

We also compared the model predictions for each species separately, to further understand which species estimates have the largest deviations. Figure 6 shows parity plots for model predictions of each species on

the ATR-FTIR data. Model estimates of nitrate and carbonate continue to decrease in accuracy at higher concentrations, when the peak overlap becomes more prevalent. Even though PLSR and PCR typically perform better than ILSR, the ILSR predictions were more accurate for carbonate, possibly because we only used a few wavelengths at the maximum heights of the nitrate and carbonate peaks, while the other models used the full spectrum. There are also large deviations for the sulfate estimates, which was expected since sulfate is present in significantly smaller concentrations compared to the other species. The baseline correction approach has also overcorrected for the area of the sulfate peak, resulting in overshooting of the model estimates.

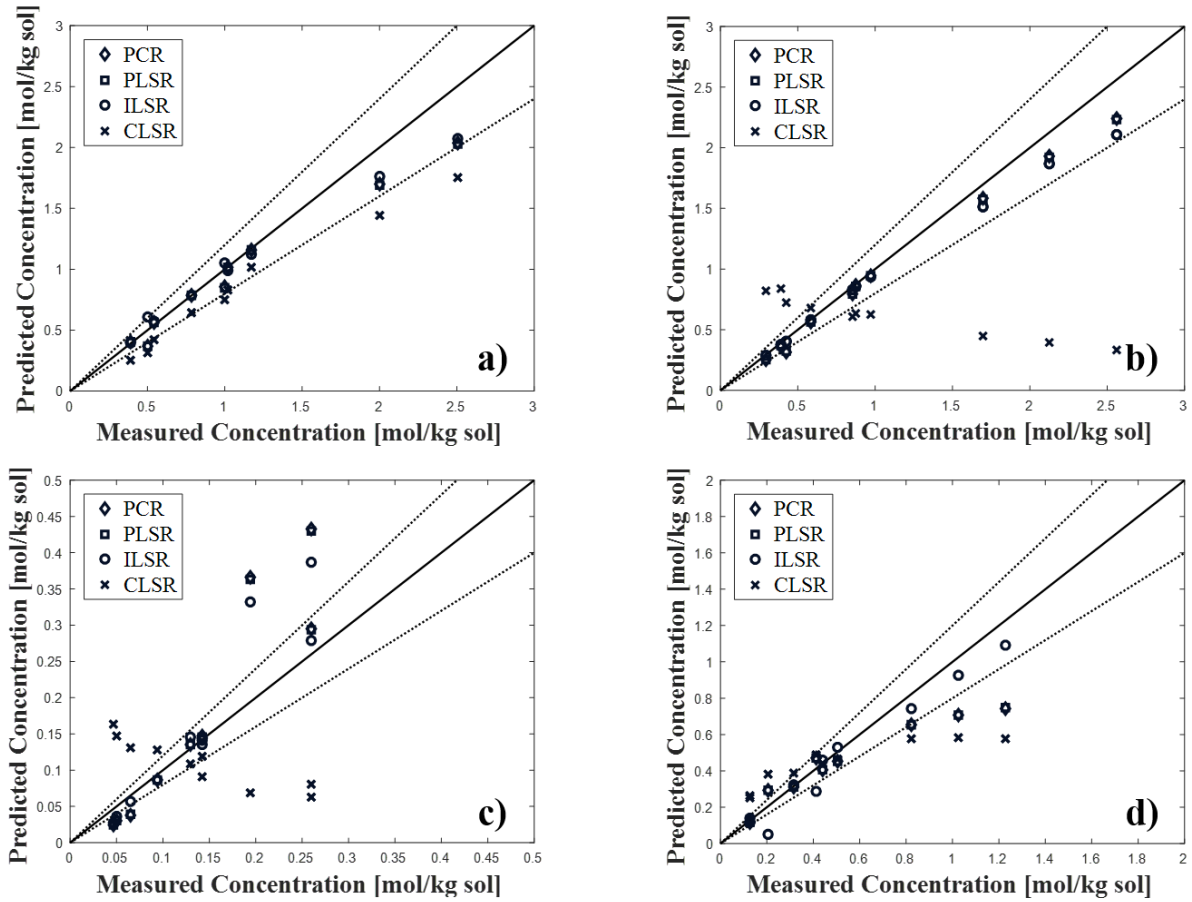

Figure 6: PCR, PLSR, ILSR and CLSR model predictions on ATR-FTIR data for a) nitrate, b) nitrite, c) sulfate and d) carbonate. The solid black line represents unity and the dashed black lines represents ±20% deviations, which are the acceptable limits at the Hanford analytical laboratory.

Model predictions on Raman data (Figure 7) follow the parity line more closely, since the peaks are sharper and the baseline effects are minimal. The PLSR and PCR models performed well within the range of the training data concentrations, indicating that the models are limited by the accuracy of the training data. Similarly to ATR-FTIR, the sulfate estimates were less accurate compared to the other species, however to a lesser extent.

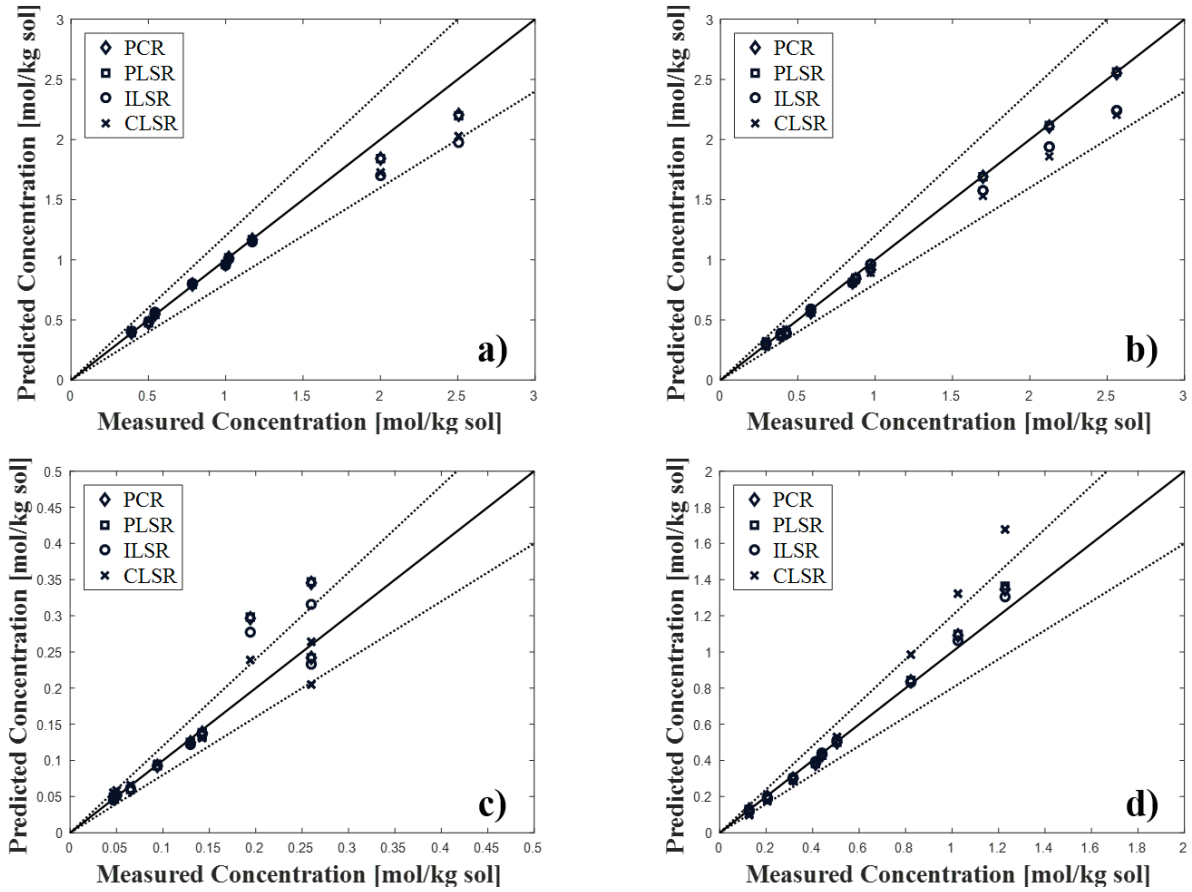

Figure 7: PCR, PLSR, ILSR and CLSR model predictions on Raman data for a) nitrate, b) nitrite, c) sulfate and d) carbonate. The solid black line represents unity and the dashed black lines represents ±20% deviations, which are the acceptable limits at the Hanford analytical laboratory.

CONCLUSIONS

Our study has revealed a few key features of ATR-FTIR and Raman spectroscopy in the context of online monitoring of salt species in nuclear waste. It is evident that the ATR-FTIR technique, characterized by larger peaks that exhibit more pronounced overlap, is more sensitive to any preprocessing steps. Our baseline correction approach needs to be revisited and optimized further to avoid overcorrection which affects the shape of the peaks and therefore the model estimates. The Raman spectra was easier to preprocess, with the exception of cosmic rays which are detected by Raman and difficult to remove, but do not affect concentration prediction as much [20].

Finally, the PLSR and PCR models generally provided the most accurate estimates of the concentrations of species, since they model the change in spectral activity as a result of the change in concentration and are thus able to deconvolute overlapping peaks more effectively. However the carbonate estimations from ATR-FTIR showed that the ILSR models gave the best prediction by using only a few key wavelengths, which shows that sometimes the simpler model may provide better estimates. ILSR is highly dependent on the wavenumber selection, so these estimates will change if different wavenumbers are selected in the calibration, while PLSR and PCR reduce the full spectrum and give more consistent predictions. Our final takeaway is that these models may not provide such accurate estimates in the presence of additional species that are not part of the training set, which is highly probable at Hanford, considering the waste is made up of many major and minor species, indicating that we cannot rely solely on calibration approaches for accurate estimates of the composition of low-activity waste.

REFERENCES

1. Wilmarth WR, Lumetta GJ, Johnson ME, Poirier MR, Thompson MC, Suggs PC, et al. Review: Waste-pretreatment technologies for remediation of legacy defense nuclear wastes. Solvent Extraction and Ion Exchange. 2011.
2. Peterson RA, Buck EC, Chun J, Daniel RC, Herting DL, Ilton ES, et al. Review of the Scientific Understanding of Radioactive Waste at the U.S. DOE Hanford Site. Environ Sci Technol. 2018;52(2):381–96.
4. Diprete CC, Howe AM. WTP Real-Time , In-Line Monitoring Program Task 2 : Determine the Technical Basis for Process Control and Task 5 : Process Control Challenges. 2017;(December).
5. Howe AM. WTP Real-Time In-Line Monitoring Program Task 1 : LAW and EMF Analytes and Properties – Functional Requirements. 2018;(March).
6. Poirier MR. WTP Real-Time In-Line Monitoring Program : Task 3 : LAW and EMF Flow Sheet Sampling Points. 2018;(March).
7. Howe AM. WTP Real-Time In-Line Monitoring Program Tasks 4 and 6 : Data Quality and Management and Preliminary Analysis Plan. 2017;(March).
8. Griffin DJ, Grover MA, Kawajiri Y, Rousseau RW. Robust multicomponent IR-to-concentration model regression. Chem Eng Sci. 2014;116:77–90.
9. Roberts JD, Caserio MC. Basic principles of organic chemistry. W.A. Benjamin; 1977. 1596 p.
10. Thomas E V., Haaland DM. Comparison of multivariate calibration methods for quantitative spectral analysis. Anal Chem. 1990;62(10):1091–9.
11. Miller JN, Miller JC. Statistics and Chemometrics for Analytical Chemistry. Pearson. 2010.
12. O'Haver T. Intro. to Signal Processing:Curve fitting B. Multicomponent Spectroscopy.
13. Jolliffe IT. Principal Component Analysis. Second Edition. Springer Ser Stat. 2002;98:487.
14. Haaland DM, Thomas E V. Partial Least-Squares Methods for Spectral Analyses. 1. Relation to Other Quantitative Calibration Methods and the Extraction of Qualitative Information. Anal Chem. 1988;60(11):1193–202.
15. Geladi P, Kowalski BR. Partial Least-Squares Regression - A Tutorial. Anal Chim Acta. 1986;185:1–17.
16. Wold S, Sjöström M, Eriksson L. PLS-Regression: a Basic Tool of Chemometrics. Chemom Intell Lab Syst. 2001;58(2):109–30.
17. Russell RL, Schonewill PP, Burns CA. Simulant Development for LAWPS Testing. 2017;(May).
18. Mazet V, Carteret C, Brie D, Idier J, Humbert B. Background removal from spectra by designing and minimising a non-quadratic cost function. Chemom Intell Lab Syst. 2005;76(2):121–33.
19. Hanrahan G, Lu K. Application of factorial and response surface methodology in modern experimental design and optimization. Crit Rev Anal Chem. 2006;36(3–4):141–51.
20. Tian Y, Burch KS. Automatic Spike Removal Algorithm for Raman Spectra. Appl Spectrosc. 2016;70(11):1861–71.

ACKNOWLEDGEMENTS

Support by the U.S. Department of Energy under Cooperative Agreement DE-FC01-06EW07053, entitled "The Consortium for Risk Evaluation with Stakeholder Participation III," is gratefully acknowledged. The authors are also thankful to Michael Stone, Richard Wyrwas, and the Real-Time, In Line Monitoring Program Group at Savannah River National Laboratory for providing the simulant recipe and useful discussions.